Seismic Testing and Performance Evaluation of Unitized Curtain Walls

Bianchi, Simona; Lori, Guido; Hayez, Valerie; Manara, Giampiero; Schipper, Roel; Pampanin, Stefano; Overend, Mauro

DOI
10.1002/eqe.70017

Publication date
2025

Document Version
Final published version

Published in
Earthquake Engineering and Structural Dynamics

Citation (APA)
Bianchi, S., Lori, G., Hayez, V., Manara, G., Schipper, R., Pampanin, S., & Overend, M. (2025). Seismic Testing and Performance Evaluation of Unitized Curtain Walls. *Earthquake Engineering and Structural Dynamics*, Article e70017. https://doi.org/10.1002/eqe.70017

Earthquake Engineering & Structural Dynamics

WILEY

RESEARCH ARTICLE OPEN ACCESS

Seismic Testing and Performance Evaluation of Unitized Curtain Walls

Simona Bianchi[1] | Guido Lori[2] | Valerie Hayez[3] | Giampiero Manara[2] | Roel Schipper[1] | Stefano Pampanin[4,5] | Mauro Overend[1]

[1]Delft University of Technology, Delft, the Netherlands | [2]Permasteelisa S.p.A., Vittorio Veneto, Italy | [3]Dow Silicones, Seneffe, Belgium | [4]Sapienza University, Rome, Italy | [5]University of Canterbury, Christchurch, New Zealand

Correspondence: Simona Bianchi (s.bianchi@tudelft.nl)

Received: 12 February 2025 | **Revised:** 12 June 2025 | **Accepted:** 26 June 2025

Funding: This study has received funding from the European Union's Horizon 2020 research and innovation programme under the Marie Skłodowska-Curie grant agreement No. 101029605 (H2020-MSCA-IF-2020–SAFE-FACE—Seismic SAFety and Energy efficiency: Integrated technologies and multi-criteria performance-based design for building FACadEs) for Simona Bianchi.

Keywords: experimental testing | fragility curves | glazed facades | seismic performance | structural silicone glazing

ABSTRACT

Unitized curtain walls are widely adopted in contemporary architecture for their lightweight construction, aesthetic qualities, ease of installation and high operational performance. They are particularly used in high-rise buildings, where glazed facades are designed to meet a broad range of performance criteria. Well-designed systems tend to perform satisfactorily in normal service conditions, but are more problematic in extreme events. In fact, post-earthquake surveys in seismic-prone regions reveal functionality losses and moderate-to-severe damage to glazed facades, with significant financial, social and environmental consequences. Despite studies on the seismic behaviour of unitized curtain walls, research in this field remains limited. In particular, experimental studies to date rarely assess both serviceability and ultimate limit states, fail to fully characterize the sequence of damage states until collapse and overlook the influence of design choices on the façade performance. To address these gaps, an extensive experimental campaign on full-scale unitized curtain walls was conducted to investigate the seismic behaviour of façade units, including variations in geometry, joint aspect ratios and type (dry-glazed or wet-glazed), frame detailing. The experiments involved quasi-static and dynamic loading, considering in-plane, out-of-plane and vertical movements. Air infiltration, water leakage and wind resistance tests were conducted before and after low-intensity shaking to assess the post-earthquake façade serviceability. Analysis of experimental data highlighted the significant influence of silicone joints on glass rotations and the structural strength hierarchy. Fragility curves were derived from damage observations, which revealed weather-tightness loss at a 0.71% drift ratio and silicone failure in specimens with low-displacement capacity frames.

1 | Introduction

Curtain walls are among the most successful and widely adopted types of façade construction. Their development at the end of the 19th century was a direct result of innovations in façade engineering, particularly by separating and suspending the façade frame from the principal load-bearing structure of the building thereby eliminating massive exterior load berating walls and ushering in the contemporary and ubiquitous curtain wall building envelope [1]. Unitized systems are increasingly preferred among the various types of glazed curtain walls. They consist of typically flat panels made of glass, aluminium, steel, natural

stone, terracotta or GFRC, connected to frames made of prismatic aluminium, steel or timber members, which are supported by the main load-bearing structure at the floor levels. Unitized systems are pre-assembled in a factory where the controlled off-site conditions ensure higher quality, shorter lead times and faster installation. Beyond ease of construction and quality of detailing, unitized systems are valued for their lightness and the ability to create expansive transparent areas. These attributes have led to their wide use in contemporary architecture, particularly in high-rise buildings.

Unitized systems cover almost the entire building envelope, accounting for 20%–30% of total building costs [2] and up to 30% of embodied carbon emissions of the building [3]. Furthermore, replacing malfunctioning glazing units in unitized façade systems has a significant impact on the cumulative embodied energy and carbon of the façade system [4]. Therefore, avoiding functional loss and damage to these components is crucial in seismic-prone countries. Beyond direct financial losses (i.e., cost of repair and replacement) and environmental impact (from repair operations and waste materials), potential damage in a glazed curtain wall façade gives rise to injuries and fatalities at street level resulting from glass falling from height and disruption to operations and services within a building arising from a malfunctioning façade. As documented in post-earthquake reports [5–7], this damage results from the vulnerability of glazed curtain walls, which are directly impacted by inter-story drift ratios and inertia forces during earthquake shaking. Initially, the seismic demand may be absorbed by the façade through internal gaps and deformations, but local stresses can concentrate in specific parts of the system, leading to damage.

Research efforts over the last decade have focused on improving the understanding of glass façade behaviour during earthquakes through analytical, experimental and numerical studies [8–10]. Initial studies [11, 12] investigated the in-plane (IP) movement and drift capacity of glass panels, identifying key deformation mechanisms: rigid body slip due to frame deflection, glass panel translation and rotation until corner bearing. These mechanisms have been consistently studied and validated through experimental tests, including monotonic, cyclic and shake table testing (e.g., [13–16]), which examined the influence of glass, clearance and connections. Comparative studies indicate that Structural Sealant Glazing (SSG) systems generally outperform dry-glazed (with mechanical restraints) systems under seismic loading, as they can accommodate greater drift before reaching equivalent damage states. However, these findings largely reflect generalized behaviour, due to the wide variability in detailing—such as gaskets, frames, glass types and connection systems—from different companies and countries. The specific influence of these design variations on façade performance remains unclear, yet understanding this is essential to inform the development of future design guidelines and enhance the seismic resilience of curtain wall systems.

Observed damage patterns include: (a) gasket or silicone degradation; (b) glass fracture; (c) glass fallout, resulting from monolithic glass cracking or failure of the glass-to-frame connection (via silicone or mechanical retention) and (d) warping of the aluminium frame, potentially leading to its partial or complete disconnection from the structure. Fragility curves have been developed to estimate damage probabilities as a function of inter-story drift [17]. However, these curves overlook serviceability losses—an essential consideration for building envelope performance following an earthquake. Arifin et al. [18] took initial steps in this direction by examining weather-tightness (e.g., water penetration) of stick curtain walls under low-intensity seismic loading. However, targeted studies on unitized curtain walls are still lacking. Furthermore, façade prototypes are rarely tested to failure, leaving their ultimate resistance and failure modes—both seismic and non-seismic—largely unknown.

Numerical simulations are widely employed by designers to support decision-making prior to prototype testing, particularly in the case of bespoke unitized curtain wall systems. Experimentally validated finite element models (FEM) and macro-models have been developed to simulate façade response (e.g., [19–22]). However, detailed modelling of connection systems—especially the non-linear behaviour of silicone in SSG systems—remains underdeveloped. Given silicone's critical role in governing the seismic performance of SSG façades, refined modelling is essential [23, 24]. Nevertheless, high-resolution experimental data required for robust model validation at façade scale remain scarce.

Based on the above discussion, this study aims to do the following:

- *Assess the impact of façade detailing on seismic behaviour*. Experimental tests were conducted on dry-glazed and wet-glazed (SSG) systems, incorporating variations in glass aspect ratios, unit configurations (vision and spandrel), joint detailing and frame properties. The comparative analysis of these design alternatives enabled the identification of key factors affecting façade response.
- *Investigate the façade performance from a holistic perspective*. The experiments aimed to assess all damage mechanisms, including non-seismic responses such as air leakage, water penetration and wind resistance, along with examining ultimate failure modes. A testing protocol was therefore devised to execute different performance tests after increasing levels of seismic intensity.
- *Detailed numerical modelling*. Advanced FEMs were developed to simulate both local (connection/joint) and global (façade-level) responses. These models were validated using high-resolution experimental data, providing a robust approach for predicting the seismic performance of unitized curtain wall systems.

As part of the EU-funded research project, these objectives were addressed through a comprehensive research program across three testing phases, as summarized in Figure 1. Phase 1 began with testing the façades to verify their seismic performance. A testing protocol was proposed involving air permeability, water resistance and wind resistance tests at increasing levels of seismic intensity. Initial data were collected for the numerical calibration of connections and overall façade behaviour. Phase 2 involved comparing dry-glazed versus wet-glazed façade systems in terms of mechanisms developing during seismic movement to accommodate inter-story drift. It also included verification of post-earthquake serviceability for higher intensity levels, seismic

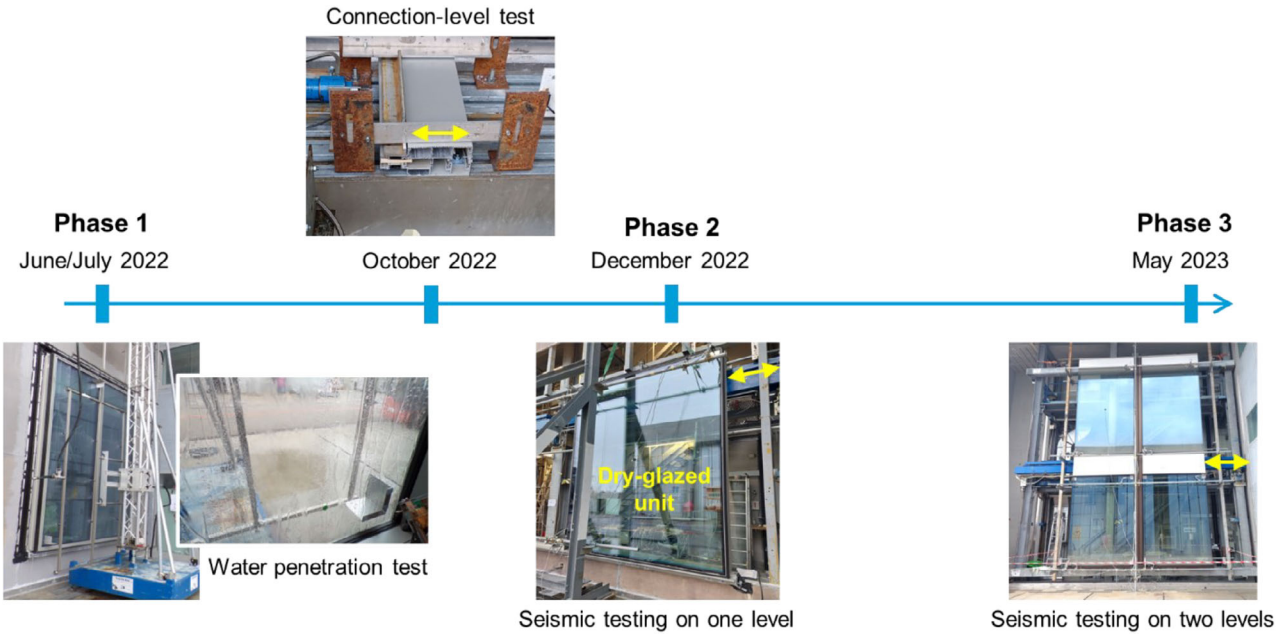

FIGURE 1 | Experimental campaign phases.

response under displacement-control cyclic and monotonic tests to study failure mechanisms. Between Phases 1 and 2, tests at the connection level were also conducted to develop specific numerical models to simulate their behaviour. Finally, Phase 3 assessed the impact of design variations on seismic response, further investigated the damage states of SSG units and compared numerical versus experimental results to capture the failure of the silicone. This paper provides an overview of the experimental tests and results, focusing on key findings derived from observations and data post-processing. It excludes the numerical studies (simplified-to-more elaborate) conducted on façade units and connection systems as part of the wider research project. Details on these numerical investigations are published elsewhere [25–27].

2 | Experiment Design

2.1 | Test Facility

The experiments were conducted at the Permasteelisa S.p.A. laboratory in Vittorio Veneto, Italy. The lab is equipped to test full-scale façades up to 10-m wide and 10-m high, including re-entrant corner configurations. These façade prototypes can be mounted on an existing two-story steel support structure framework with upper and lower fixed beams and an intermediate moving blue beam (Figure 2a). This 'seismic beam' can be subjected to a maximum displacement of ±150 mm in the IP horizontal (X) direction, ±50 mm in the IP vertical (Y) direction and ±45 mm in the out-of-plane (OOP) (Z) direction by means of hydraulic actuators. These actuators are connected to a digital controller and a control panel to facilitate the application of desired displacements in both quasi-static and dynamic loading sequences, with frequencies ranging from 0.25 to 1 Hz.

The facility enables testing in two different layouts (Figure 2b). Layout A is designed for experiments on single-storey glazed units or units arranged in a row. This layout allows for the analysis and comparison of façade configurations subject to the same loading type. Layout B is intended for testing façades across two floor levels. In Layout B, the seismic beam is located at the intermediate floor level; consequently, this does not replicate real-world scenarios where inter-story drift ratios vary from one floor level to another. Rather, it is commonly used in performance tests to assess the movement of the façade at the horizontal joint between vertical units and verify compliance with project requirements (e.g., maximum allowable movement). Both layouts were considered during the experiments.

2.2 | Façade Prototype Details

Two unitized curtain wall systems (T1 and T2), each representing a real-world bespoke façade project, were tested in the experimental campaign using units in their original configurations or with targeted design variations, as summarized in Table 1. The first system (T1) included two SSG units (T1-1), each measuring 3430 mm in height and 1267.5 mm in width, and one dry-glazed unit (T1-2), measuring 3430 mm × 2535 mm. After initial testing, the dry-glazed unit was reglazed into an SSG configuration—by replacing mechanical restraints with a silicone joint—resulting in a wider SSG unit (T1-3). The second system (T2) consisted of four SSG units as follows: T2-1 and T2-2 measured 3850 mm × 2250 mm, while T2-3 and T2-4 measured 4612.5 mm × 2250 mm. T2-3 retained the original silicone dimensions (27 × 9 mm), while the others incorporated variations in silicone joint geometry to assess the impact of aspect ratio on seismic performance. Silicone joint dimensions were selected based on simplified numerical modelling of façade response, as discussed in Hayez et al. [24]. In total, seven different units were examined, enabling a broad comparison of seismic performance across variations in glass size, spandrel layout and joint detailing.

Each façade system was designed in accordance with project-specific requirements and relevant codes, including EN 1998-1

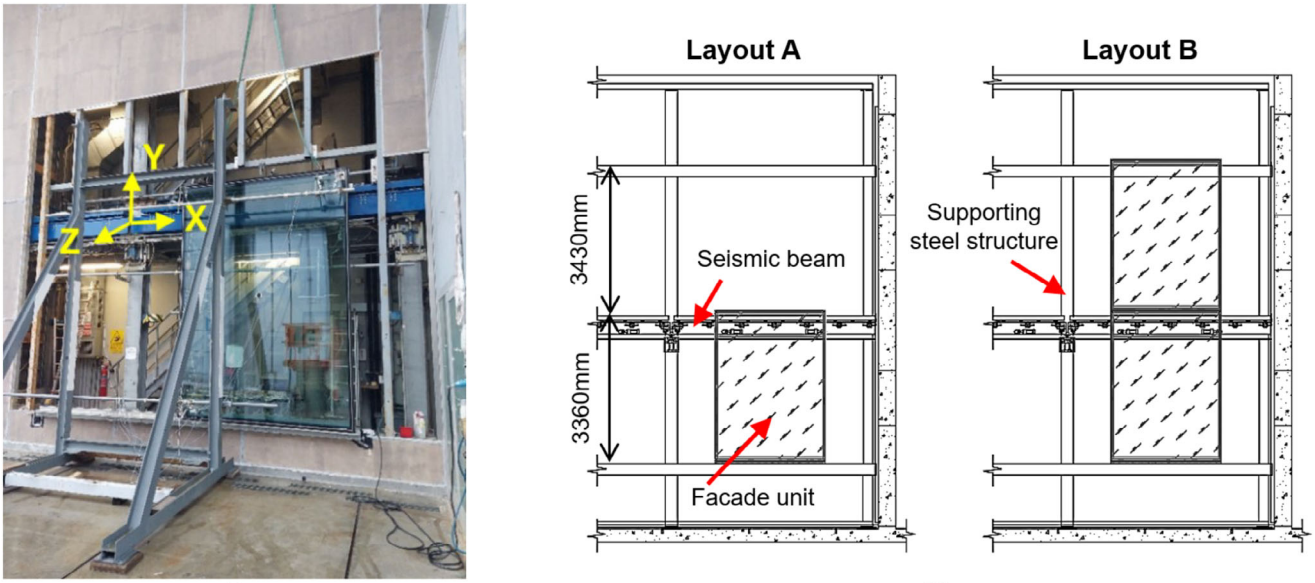

FIGURE 2 | (a) Facade specimen installation and seismic movement directions. (b) Layout configurations.

TABLE 1 | Façade unit configurations.

Façade unit	Unit config.	Unit height [mm]	Unit width [mm]	Unit aspect ratio	Glass aspect ratio	Joint config.	Silicone bite [mm]	Silicone width [mm]	Silicone aspect ratio
T1-1	Original	3430	1267.5	2.71	2.71	SSG	25	8	3.13
T1-2	Original	3430	2535	1.35	1.35	Dry	—	—	—
T1-3	Modified	3430	2535	1.35	1.35	SSG	25	8	3.13
T2-1	Modified	3850	2250	1.71	1.35	SSG	20	9	2.22
T2-2	Modified	3850	2250	1.71	1.35	SSG	9	9	1.00
T2-3	Original	4612.5	2250	1.84	1.64	SSG	27	9	3.00
T2-4	Modified	4612.5	2250	1.84	1.64	SSG	9	9	1.00

[28] for seismic demand, UNI EN 13830 [29] for testing protocols, JASS14 [30] for deformation verification and EAD 090010-00-0404 [31] for silicone joint design. Connection details were specifically designed to accommodate multi-directional seismic displacements and were consistent across all configurations (Figure 3a). The façade framing consisted of aluminium (type 6063 T6) extruded profiles, with mullions and transoms connected via screws. Mullions of different units were linked using male–female joints incorporating thermal breaks and anti-buckling components. The starter sill was connected to the bottom transom of the units through screwed alignment blocks and shear keys. The units were equipped with stack joints for vertical movements, and gaps in mullions and transoms to enable horizontal IP movement through panel racking and frame distortion.

One façade system (T1-2) consisted of a dry-glazed configuration with gaskets and mechanical restraints in the connections, while the other facades had DOWSIL 993 structural silicone as the bonding element between the frame and glass across all units. The glass panels were supported by their setting blocks, used to carry their weight and to maintain their position within the curtain wall frame. Unit T1 included triple-glazing panels, with the two smaller units (T1-1) also featuring an operable joint for a top-hinged window, while unit T2 consisted of double-glazing panels. The façade was connected to the main structure by means of hooks, brackets and adjusting bolts. Each unit had two hooks for the upper bracket anchored to the steel beam and fixed connections for the bottom bracket (Figure 3b). The hooks had different constraints in the horizontal IP direction: one hook was fixed using screws, while the other hook was free to move. This constraint scheme allows the unit to accommodate differential thermal and building movements. The hooking connections also enable to absorb the horizontal OOP seismic movement through rotation and can accommodate construction tolerances. Vertical tolerance is achieved through adjusting bolts, while horizontal tolerance is provided by the clearance between the hook and the steel plate (Figure 3b).

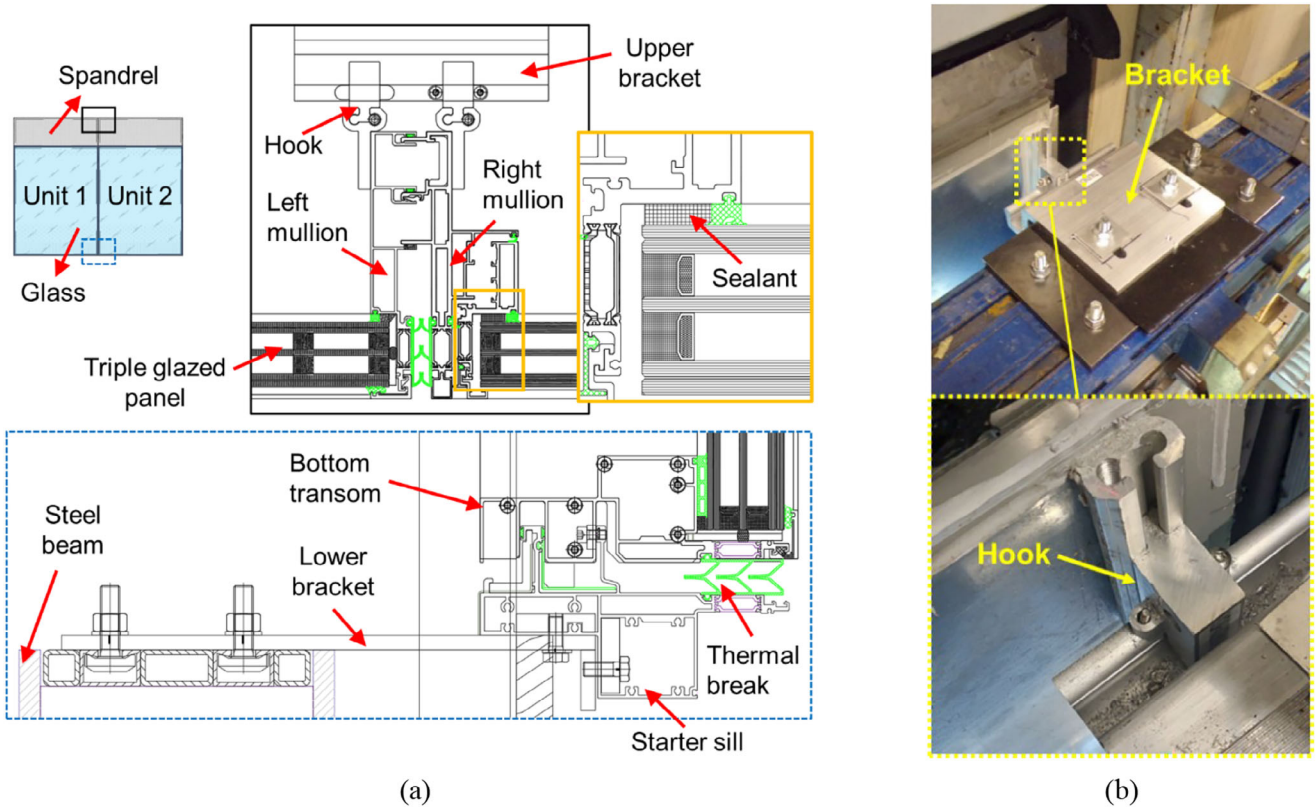

FIGURE 3 | Construction details of the facade specimens (a) and connection system to the seismic beam (b).

An additional variation was introduced to T2 unit frames during testing. In the *Original* configuration, the frame was designed to accommodate seismic movements while protecting the silicone joints from damage. This was achieved by inserting an angular steel plate into the alignment screw connection, preventing contact with the starter sill and avoiding early horizontal sliding of the bottom transom at low drift levels, as observed by Galli [32]. This solution allowed for greater relative vertical displacement of the bottom transom with respect to the starter sill. *Modified* configurations were also tested for all T2 units, featuring restrained bottom transoms that limited rotation and significantly reduced the deformation capacity of the frame. In addition, unit T2-2 introduced a further variation: to simulate sealant defects along the glass–frame interface, progressive cuts—up to 80% of the total silicone length—were made around the perimeter. This aimed to evaluate the influence of crack propagation on seismic performance during subsequent testing of the intentionally damaged unit, as discussed in the next section.

2.3 | Instrumentation Layout

An instrumentation layout was designed for each configuration to capture the IP and OOP movements of the glass, frame and unit connections during seismic loading (Figure 4). The monitoring system comprised 31 displacement sensors, including potentiometers and LVDT transducers with strokes of 50, 100 and 200 mm. These sensors recorded vertical and horizontal (absolute) displacements of the glass panels and frame system, including the mullion-bracket connections to the seismic beam. The recorded displacements enabled the assessment of glass panel rotations, as well as frame rotations, distortions and diagonal elongations. Four draw wires with a 50-mm measurement range were used to monitor diagonal and corner elongations of the unit frame. Three laser sensors with detection ranges of 200 and 500 mm tracked the movement of the seismic beam. Additionally, 4–6 accelerometers (±6 g) measured accelerations on the glass panels and bracket connections, while strain gauges recorded strains on the glass (near the setting blocks), on a bottom mullion-transom joint of the frame and on an upper bracket. Videos were recorded using GoPro and other digital cameras to capture both the front view and the local behaviour at bracket connections. Cameras were positioned to capture silicone joint movements in specimens T2 (1–4). Adhesive rulers were attached around the perimeter to monitor relative displacement and potential crack propagation through visual inspections and crack width measurements. Beyond video recordings, cameras also captured repeated scans and point clouds at key locations on the glass and silicone to support Digital Image Correlation analysis.

All strains, deformations and accelerations were acquired using the same data acquisition device and controller, with calibration factors applied to ensure measurement accuracy of sensors. All data were collected at a sampling frequency of 200–1000 Hz to provide a sufficient sample size for filtering during post-processing. A Butterworth low-pass filter was applied to all recorded acceleration data to remove noise outside the range of interest.

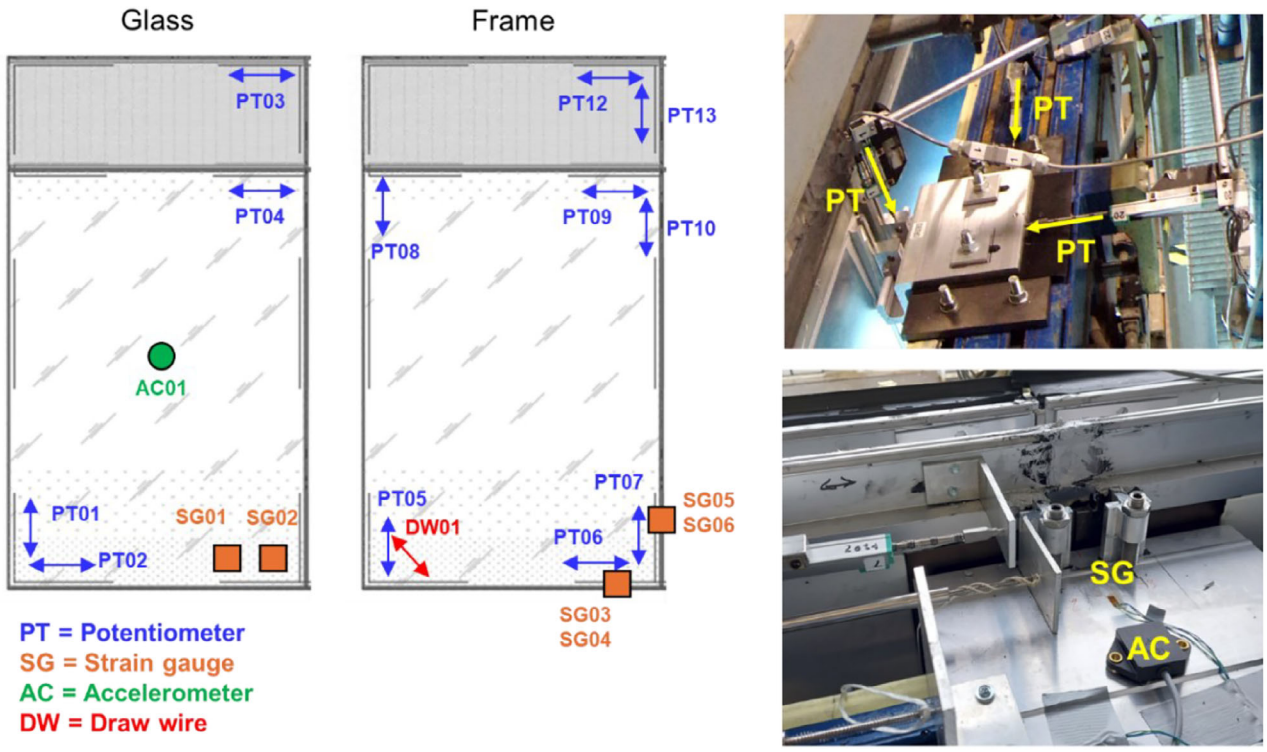

FIGURE 4 | Instrumentation layout for the glass panel, internal framing and bracket connection of a façade unit.

2.4 | Test Protocol

The following seismic loading types were adopted in the campaign:

- Cyclic tests: These tests, conducted following JASS14 [30] and UNI EN 13830 [29], aimed to verify compliance with certification standards by assessing the façade's capacity to withstand seismic demands without significant damage. Seismic displacements were applied separately in all directions (*X*-horizontal IP, *Y*-vertical IP, *Z*-horizontal OOP). These tests involved 10 cycles with maximum IP displacements of 0.36%, 0.71% and 1.10% drift ratio, and half these values in the vertical direction, with a signal frequency range of 0.24–0.45 Hz. The drift ratios were selected based on the performance checks provided by the JASS14 [30], which indicates values of H/300 (no damage to internal and external components), H/200 (external components must not exceed allowable stress, and sealing must be repaired) and H/100 (no damage to the glass or dropout of any component is allowed).
- Crescendo tests: Designed to exceed typical design limits, these tests aimed to identify damage initiation, progression and drift capacity of the façades under increasing cyclic demands. Following AAMA 501.6 [33], these experiments involved a series of sinusoidal cycles consisting of a succession of four cycles of ramp up intervals followed by four cycles of constant amplitude intervals (Figure 5a), with displacements ranging from 0.36% to value of 2.10% drift, corresponding to the maximum achievable by the test facility, with frequencies at 0.4 and 0.8 Hz.
- Earthquake records: To simulate realistic earthquake sequences (dynamic loading) and investigate their impact on façade damage modes, two far-field (Friuli 1976 earthquake—Peak Ground Acceleration (PGA) = 0.11 g, Soil Type C, Station ST33; and Umbria-Marche 1997 earthquake—PGA = 0.17 g, Soil Type C, Station ST223) and one near-fault (Christchurch 2011 earthquake—PGA = 0.17 g, Soil Type D, Station CCCC) records were selected from a set of spectrum-compatible earthquakes. The testing protocol involved applying inter-story drift time series generated through non-linear dynamic analysis of a multi-story reinforced concrete building designed according to the NTC 2018 [34] for a high-seismicity zone (PGA = 0.33 g), as described in Ciurlanti et al. [35]. The records, with floor response spectra for a specific intensity level shown in Figure 5b, were scaled to reach maximum drift amplitudes of 0.71% and 1.10%, according to the cyclic tests. Testing was conducted in the primary *X*-horizontal direction, as well as using combined *XY*-horizontal and vertical motion (synchronized horizontal–vertical movement).
- Monotonic tests: These tests were performed to identify ultimate failure modes and mechanisms of façade units by reaching higher drift levels than those in cyclic and dynamic tests. Horizontal IP tests were conducted up to a maximum displacement of 250 mm (7.4% drift), at 0.5 mm per second, corresponding to the maximum capacity of the testing facility. After each loading step (every 50 mm), testing was temporarily halted for visual inspection of the façade, with particular attention to the silicone joint.

Eight façade specimens, comprising different unit combinations (T1, T2), were tested across multiple phases using the outlined protocols. This experimental campaign resulted in approximately 140 seismic tests, including repeated tests at various intensity levels, as summarised in Table 2. Phases 1 and 2 testing also

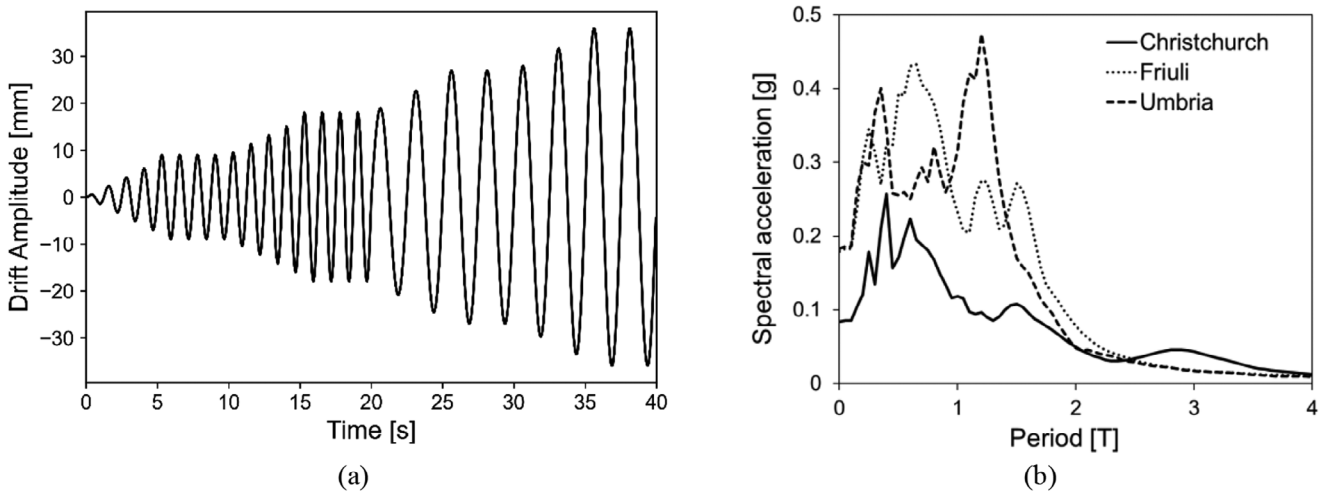

FIGURE 5 | (a) Crescendo input until 1.10% drift ratio. (b) Floor response spectra at 1.10% drift ratio.

included assessments of air infiltration, water leakage and wind resistance, conducted before and after the seismic tests to evaluate the post-earthquake serviceability of the façade (Table 3). These tests were performed in the same test chamber through the installation of wooden panels (partly shown on the mock-up in Figure 2a) connected to the glazed units by a waterproofing sheet to make the full mock-up airtight. The air infiltration test was conducted under static pressure to determine air leakage through the façade specimen at differential pressures up to 600 Pa, in accordance with EN 12153 [36]. The water penetration test involved applying a differential pressure (up to 900 Pa) across the curtain wall assembly while simultaneously spraying water on the exterior façade surfaces, following EN 12155 [37]. For the wind resistance test, both serviceability and safety requirements were assessed, with wind load amplified by a safety factor of 1.5. Positive and negative pressure increments were applied to the specimen, reaching pressures of 1500 Pa for pressure and 1900 Pa for suction, before reducing the pressure to zero, as prescribed in EN 12179 [38]. Due to the presence of openings in the T1-1 units, an air permeability test was also conducted after applying self-adhesive sealing tape to the internal perimeter of the frame (simulating the absence of the opening) to investigate their impact.

3 | Experimental Results

3.1 | Demand on Façade Components

The experimental data were processed to derive the seismic demand experienced by different façade components, through sensors located on the glass panels, internal frame and bracket connections. When the façade specimens were subjected to IP seismic movements driven by drift amplitudes, a combined racking and rocking motion was triggered, characterized by the rigid translation and rotation of the façade. The vertical stack joint along the transoms accommodated the resulting upward and downward differential movements, with the glass panels rotating on their setting blocks. As the frame began to deform at higher drift levels and its male–female mullions slipped vertically relative to each other, the unit assumed a rhomboidal shape (Figure 6a), increasing the risk of contact between the glass edge and the aluminium frame, and stress was introduced into the joints to accommodate the inter-story drift.

However, further analyses of the positive/negative *X* directions showed that the rotation of the glass differed between the two directions, and sliding of the glass on its support blocks was also recorded. As highlighted in a previous study by Galli [32], this behaviour results from the asymmetric restraint conditions of the unit and the alignment screw/block in the bottom transom, used to adjust the position of the façade units during installation and acting as a restraint on horizontal translation. This leads to a movement that favours rotation more in one direction (Figure 6b). The rhomboidal deformation, more pronounced in the opposite direction, is likely the most hazardous to the integrity of the glass components and must be carefully considered. Rotational movements, on the other hand, help prevent excessive unit deformation and reduce the risk of glass–frame contact and fracture. When the façade was subjected to OOP movements, the unit rotation was facilitated by the clearance in the sill/transom and primarily governed by the hinge at the hook-bracket connection, while the SSG joints remained unstrained by such movement.

The displacement values recorded by the sensors were used to derive the following demand parameters from geometrical considerations: (i) rotation of the glass, measured relative to its diagonal; (ii) rotation of the frame (when compared to the diagonal), distortion of its corners and frame diagonal elongation (Figure 6c). Considering all the SSG units and focusing on the same intensity level (0.71% drift ratio, equivalent to 24-mm drift amplitude for the X-IP and Z-OOP horizontal movements, while equal to half this value–12 mm—for the *Y* vertical shaking), the overall demand parameters (i.e., the mean of absolute maximum recorded values for the same loading) are compared and summarized in Tables 4 and 5. Moreover, the acceleration of glass and brackets was also derived from the sensor recordings. Strain values were instead measured for certain units, (T2-1–4), by means of strain gauges placed at strategic locations as discussed above. By assuming strength values of 40 MPa, 160 and 355 MPa for the glass, aluminium frame and steel brackets, respectively, utilization factors were calculated by converting

TABLE 2 | Test matrix.

Phase	Specimen	Layout	Description (unit type, floor level)	N. tests	Loading type (direction Drift ratio)
1	1	A	2 units of type T1-1, first level	4	Cyclic (*X*–0.36%, 0.71%)
				3	Cyclic (*Z*–0.36%, 0.71%)
	2	A	2 units of type T1-1 and 1 unit of type T1-2, first level	3	Cyclic (*X*–0.36%, 0.71%)
				2	Cyclic (*Y*–0.18%, 0.36%)
				2	Cyclic (*Z*–0.36%, 0.71%)
2	3	A	2 units of type T1-1 and 1 unit of type T1-3, first level	3	Cyclic (*X*–0.36%, 0.71%)
				2	Cyclic (*Y*–0.18%, 0.36%)
				2	Cyclic (*Z*–0.36%, 0.71%)
	4	A	1 unit of type T1-3, first level	4	Crescendo (*X*–0.36%, 1.40%)
				2	Monotonic (*X*—Up to 7.4%)
3	5	B	1 unit of type T2-1 and 1 unit of type T2-2, first level + 1 unit of type T2-3 and 1 unit of type T2-4, second level	5	Crescendo (*X*–0.71%, 0.95%, 1.10%)
				7	Earthquake (*X*–0.71%, 1.10%)
				7	Earthquake (*XY*–0.71%, 1.10%)
				4	Crescendo (*Y*–0.36%, 0.71%)
	6	A	1 unit of type T2-1 and 1 unit of type T2-2, first level	3	Crescendo (*X*–0.71%, 1.10% and 2.10%)
				2	Earthquake (*X*–0.71%, 1.10%)
				11	Monotonic (*X*—Up to 6.7%)
	7	A	1 unit of type T2-1 and 1 unit of type T2-2 (with cuts in silicone), first level	35	Crescendo (*X*–0.71%, 1.10%, 1.4%, 1.8%, 2.10%)
				1	Monotonic (*X*—Up to 5.9%)
				5	Crescendo (*X*–0.71%, 1.10%, 1.4%, 1.8%, 2.10%)
				1	Monotonic (*X*—Up to 5.9% drift)
				15	Crescendo (*X*–0.71%, 1.10%, 1.4%, 1.8%, 2.10%)
				1	Monotonic (*X*—Up to 5.9%)
	8	A	1 unit of type T2-3 and 1 unit of type T2-4, first level	4	Earthquake (*X*–0.71% and 1.10%)
				5	Crescendo (*X*–0.71%, 1.10%, 1.4%, 1.8%, 2.10%)
				1	Earthquake (*X*–2.9%)
				1	Monotonic (*X*—Up to 6.7%)

strains (ε, recorded from strain gauges) into stresses ($\sigma = E \cdot \varepsilon$, with E Young's modulus of glass/frame at 70 GPa and steel at 210 GPa).

Initial observations can be made by analysing the demand parameters on the different façade components summarized in the previous tables (where no values indicate that either the specific parameter was not recorded during the tests or errors occurred in the measurements). Comparing the glass and frame responses in different directions (*X*, *Y*, *Z*) under cyclic loading—the only loading type where all directions were tested—it is evident that

- rotations due to vertical IP loading (*Y*) are low when compared to the other directions, with the frame having twice the rotation value obtained for the glass;
- OOP rotations are approximately twice as high as IP rotations, due to the higher flexibility of the façade to accommodate wind loading. The frame rotations always exceed those of the glass except for T1-1, where the high aspect ratio (2.71) resulted in increased rocking motion of the glass on its setting blocks;
- the impact of vertical loading on the frame diagonal elongation is particularly noticeable;

TABLE 3 | Test sequence including serviceability check.

Test	Configuration	Description
1	Pre-seismic	Air permeability test (600 Pa)
2	Pre-seismic	Water penetration test (900 Pa)
3	Pre-seismic	Wind resistance (1500 and 1900 Pa)
4	Seismic, Intensity 1	Cyclic (X, ±0.36% drift, 10 cycles)
		Cyclic (Z, ±0.36% drift, 10 cycles)
		Cyclic (Y, ±0.18% drift, 10 cycles)
5	Post-seismic, Intensity 1	Air permeability test (600 Pa)
6	Post-seismic, Intensity 1	Water penetration test (900 Pa)
7	Seismic, Intensity 2	Cyclic (X, ±0.36% drift, 10 cycles)
		Cyclic (Z, ±0.36% drift, 10 cycles)
		Cyclic (Y, ±0.18% drift, 10 cycles)
8	Post-seismic, Intensity 2	Air permeability test (600 Pa)
9	Post-seismic, Intensity 2	Water penetration test (900 Pa)
10	Post-seismic, Intensity 2	Wind resistance (2250 and 2850 Pa)

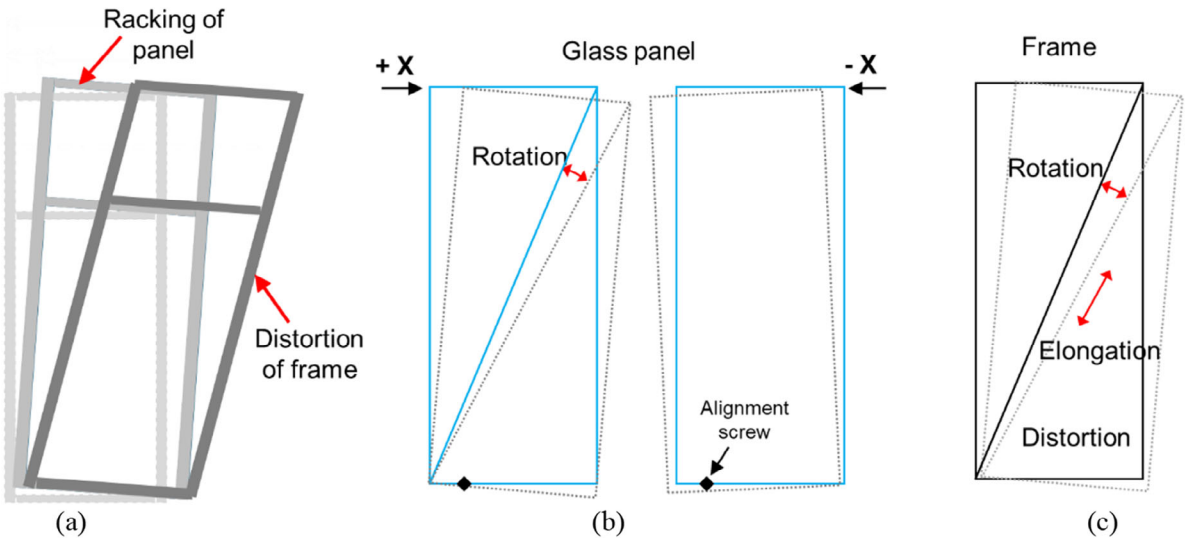

FIGURE 6 | (a) Seismic behaviour of the façade unit; (b) glass rotation and asymmetric behaviour of the panel; (c) frame performance indicators (rotation, diagonal elongation, distortion).

- distortion values in the frame corners increase under dynamic loading, with higher recorded values (93.3°) observed for the T2-4 façade under the highest earthquake intensity (Friuli at 100-mm maximum displacement).

Across the different displacement records, residual displacements were found to be negligible for the frame, indicating that the component behaved within the elastic domain throughout all the low–moderate intensity tests (up to 100 mm), and the relative displacements between the glass and frame remain within the internal gap dimensions (8 mm). Moreover, when comparing the results across the different façade units with the same loading type, it can be observed that glass behaviour is especially affected by the joint properties. As discussed below, the higher flexibility of lower aspect ratio silicones (9 × 9) led to increased glass rotations, with higher values associated with the higher unit aspect ratio (Figure 7a). Through statistical and regression analysis of data (as shown in Bianchi et al. [39]), it is also observed that the glass rotation increases by about 20% with its aspect ratio, frame diagonal elongation decreases linearly by about 40% with increasing unit aspect ratio, while no specific trends can be observed in frame distortions and rotations, characterized by a wide dispersion in the data points.

Regarding acceleration values, the glass panels showed a maximum amplification factor of 1.7 due to the unit flexibility and glass rocking behaviour. This factor was determined by comparing the glass accelerations with that at the bracket connected to the seismic beam. Both glass and frame exhibited low utilization factors

TABLE 4 | Demand parameters for the glass panels (max seismic beam displacement of 24 mm for *X* and *Z* direction, 12 mm for *Y* direction).

Façade unit	Loading type	Horizontal IP displ. [mm]	Horizontal OOP displ. [mm]	Vertical displ. [mm]	IP rotation [°]	OOP rotation [°]	Acceleration [g]	Utilization factor [%]
T1-1	Cyclic X	23.10	1.62	3.90	0.30	0.03	0.41	1.90
	Cyclic Y	1.20	1.21	12.10	0.07	0.02	0.26	0.54
	Cyclic Z	0.30	25.61	3.05	0.02	0.50	0.66	—
T1-3	Cyclic X	24.15	1.41	2.49	0.33	0.02	0.49	3.68
	Cyclic Y	2.70	2.22	9.68	0.03	0.04	0.24	1.84
	Cyclic Z	1.20	37.52	3.29	0.02	0.62	0.71	3.40
T2-1	Crescendo X	14.80	—	1.20	0.13	—	0.31	2.58
	Earthquake X	12.67	—	6.40	0.14	—	0.55	3.04
	Earthquake XY	12.10	—	9.53	0.15	—	0.44	2.26
T2-2	Crescendo X	19.40	—	0.40	0.18	—	0.61	4.16
	Earthquake X	16.58	—	0.93	0.16	—	0.79	3.85
	Earthquake XY	12.37	—	5.77	0.14	—	—	5.11
T2-3	Crescendo X	10.10	—	1.50	0.11	—	0.55	—
	Earthquake X	9.30	—	1.67	0.10	—	0.66	—
	Earthquake XY	12.52	—	2.42	0.15	—	0.56	6.56
T2-4	Crescendo X	19.50	—	0.70	0.24	—	—	—
	Earthquake X	18.03	—	0.77	0.22	—	—	—
	Earthquake XY	16.94	—	0.81	0.20	—	—	—

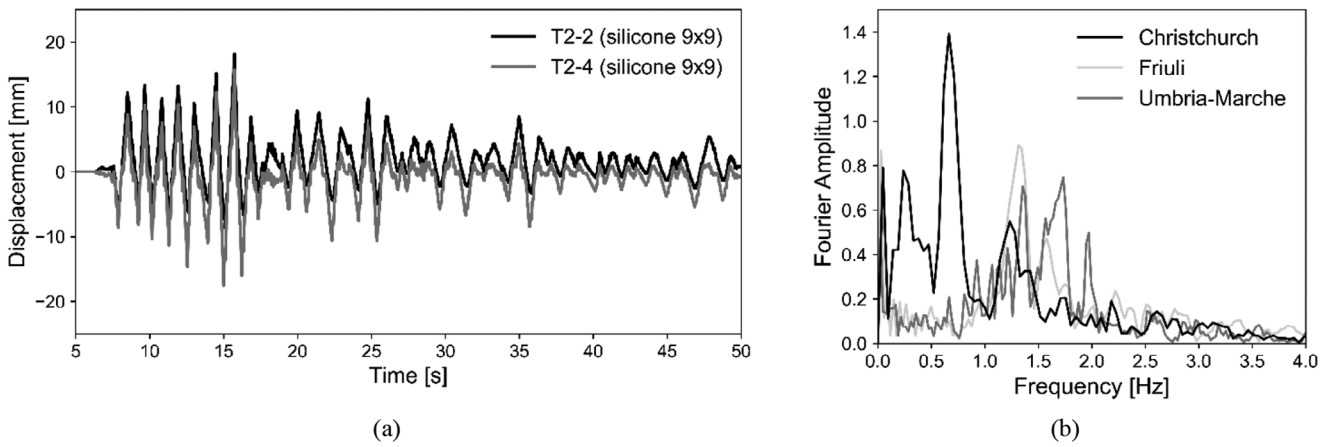

FIGURE 7 | (a) Example of recording for the glass horizontal displacement for the panels with lower silicone aspect ratio (9 × 9) for the same input (Umbria–24 mm, 0.71% drift ratio); (b) Fourier amplitude spectra for the three earthquakes at 0.71% drift ratio.

(below 10% across all intensities), with higher values recorded during earthquake dynamic loading and in scenarios with limited frame displacement capacities (*Modified* frame configuration). During the Crescendo tests at 72 mm for specimens T2-1 to T2-4, utilization factors reached up to 18.4% for the transom and 31.8% for the bracket connection. For monotonic tests, a 15-fold decrease was found in the bracket's utilization factor as expected for quasi-static loading. This highlights the critical role of acceleration at the bracket level, compared to displacement seismic demand.

Upon further analysis of the data comparing results from different loading types, it was observed that the maximum recorded values across various sensors remained consistent at different intensity levels. However, the dynamic effect on the façade became evident when comparing cyclic and dynamic responses, with the time-history loading causing displacements in the various components that were nearly 1.5 times lower than those recorded in cyclic testing. This can be attributed to the damping properties of the silicone and internal gaps affecting the distribution of loads into the components. When comparing

TABLE 5 | Demand parameters for the aluminium frame (max seismic beam displacement of 24 mm for *X* and *Z* direction, 12 mm for *Y* direction).

Façade unit	Loading type	Horizontal IP displ. [mm]	Horizontal OOP displ. [mm]	Vertical disp. [mm]	IP rotation [°]	Distortion [°]	Diagonal elongation [mm]	OOP rotation [°]	Utilization factor mullion [%]	Utilization factor transom [%]
T1-1	Cyclic X	19.98	3.10	5.95	0.28	90.30	4.41	0.05	—	—
	Cyclic Y	1.62	2.50	12.30	0.13	91.11	21.74	0.04	—	—
	Cyclic Z	1.90	21.88	2.05	0.01	90.20	3.03	0.37	—	—
T1-3	Cyclic X	19.73	1.50	10.8	0.40	90.91	18.78	0.03	4.24	3.85
	Cyclic Y	2.60	1.30	20.15	0.08	90.79	18.33	0.02	2.63	2.84
	Cyclic Z	0.50	34.90	3.39	0.02	90.15	4.61	0.58	2.93	1.75
T2-1	Crescendo X	19.60	—	4.40	0.29	91.05	3.19	—	—	—
	Earthquake X	15.55	—	3.52	0.18	90.24	4.05	—	—	—
	Earthquake XY	12.80	—	8.20	0.20	90.60	12.51	—	—	—
T2-2	Crescendo X	20.50	—	4.30	0.32	91.25	13.37	—	2.37	2.64
	Earthquake X	16.90	—	2.63	0.20	90.29	3.36	—	2.16	2.89
	Earthquake XY	14.67	—	7.93	0.22	90.52	11.14	—	2.55	2.58
T2-3	Crescendo X	15.60	—	8.00	0.22	90.52	3.72	—	—	—
	Earthquake X	12.43	—	2.10	0.19	90.48	5.25	—	—	—
	Earthquake XY	14.47	—	6.31	0.21	90.35	4.35	—	1.30	5.05
T2-4	Crescendo X	17.44	—	2.80	0.24	90.22	2.56	—	—	—
	Earthquake X	13.65	—	4.26	0.20	90.19	4.35	—	—	—
	Earthquake XY	15.05	—	8.59	0.21	90.33	3.64	—	1.40	4.39

the results between the Crescendo and time-history tests, the latter showed slightly reduced displacements in the order of 1.1–1.2 times across all the façade specimens, with the frequency content impacting the seismic demand on the façade components. The near-field earthquake (Christchurch) is characterized by higher accelerations and limited frequency content, while the far-field earthquakes (Friuli and Umbria–Marche) exhibit higher frequencies, as can be observed from the Fourier amplitude spectra of Figure 7b. This results in higher displacements for the Christchurch earthquake, where the facades are more vulnerable to low-frequency vibrations. At higher intensities, a slight shift and increase in amplitude at lower frequencies were observed for the Umbria and Marche earthquakes due to energy redistribution to these lower frequencies. This behaviour can be attributed to the facade's flexibility, which can accommodate displacements without transferring excessive forces back to the structure.

3.2 | Impact of Glass–Frame Joints

The results provide insights into the behaviour of dry-glazed versus wet-glazed units by directly comparing the responses of T1-2 and T1-3, with the latter designed to replicate an SSG configuration equivalent to T1-2. Post-processing the sensor data reveals that the SSG unit exhibits higher rotations under IP loading (Figure 8a). This is due to the flexible silicone joints and their redistribution of seismic forces across the façade, allowing for greater movement compared to the more rigid connections found in dry-glazed systems, which use mechanical fixings such as gaskets and pressure plates. On the other side, this flexibility in SSG connections results in increased distortion and diagonal elongation of the frame, to be considered in the design due to its potential impact on panel misalignments and increased connection stresses at higher drift levels. Higher rotations of the SSG unit are also observed in the OOP loading direction. Distortions and diagonal elongations are instead higher for the dry system under vertical *Y* loading due to its direct transfer through the mechanical connections, with the internal gaps in the joint facilitating the movement.

In general, SSG systems typically exhibit superior performance compared to other glazing systems. This is also confirmed by fragility data collected from past experimental testing, showing that SSG solutions can withstand higher seismic demands before reaching the same level of damage as dry-glazed systems [17, 40]. It is observed that a dry-glazed system with mechanical caps can lead to glass fracture when subjected to inter-story drifts, as they introduce local hard-spots and lack the continuous attachment found in SSG systems. In contrast, SSG joints effectively prevent glass fracture during low-to-moderate

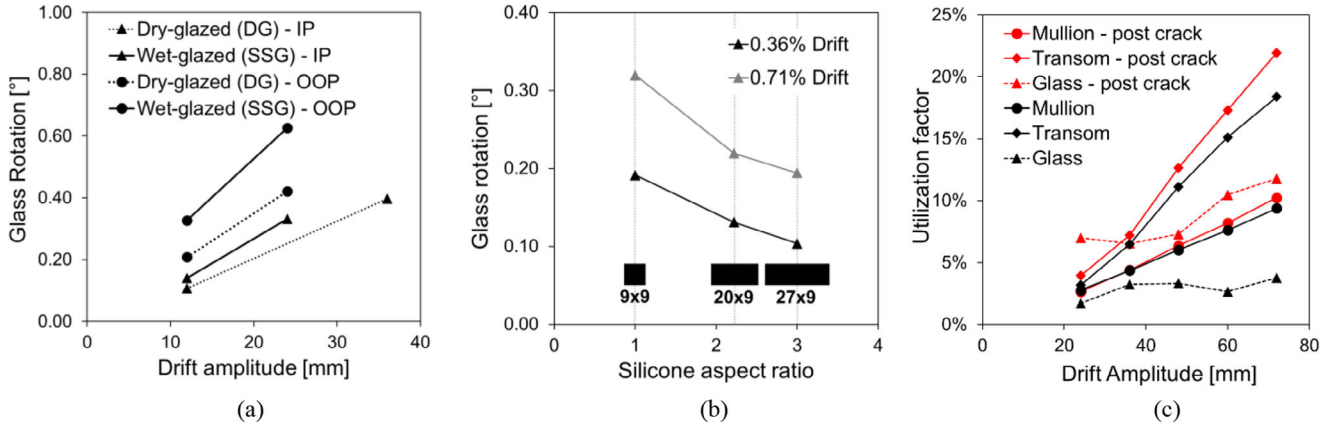

FIGURE 8 | (a) Comparison of dry-glazed (DG) versus wet-glazed (SSG) response in terms of glass rotations (IP X-loading and OOP Z-loading). (b) Glass rotations (mean values) versus silicone aspect ratio at two different seismic intensity levels. (c) Utilization factors in the frame and glass before/after cracks in the silicone of Façade 5-T2 at increasing (max) drift amplitudes during the Crescendo tests.

earthquakes by securely connecting the glass panel to the frame using a structural sealant, thereby reducing the risk of hard contact between the glass and aluminium surfaces. However, correct joint dimensions are critical to fully harness the benefits and effectively transfer seismic forces to accommodate imposed movements.

Depending on the adhesive properties and joint dimensions, SSG systems can meet seismic performance requirements associated with various damage levels. For this reason, different SSG joints were explored during the tests. Adjusting the silicone dimensions allowed investigation into the potential influence of joint aspect ratio, given that lower aspect ratios can enhance movement capability. It was indeed observed that the silicone dimensions particularly impacted the horizontal glass displacement, leading to smaller glass rotations with increasing silicone aspect ratios. As discussed in Bianchi et al. [39], this was especially evident when the aspect ratio increases from 1.00 to 2.22, where a 30% decrease was observed, whereas the glass rotation remained unaffected for higher values—between a 2.22 and 3.00 silicone aspect ratio (Figure 8b). Although the lower silicone aspect ratio (1.00) led to higher displacements, no additional damage or crack propagation was observed in the T2-2 unit, where artificial cuts were introduced to simulate an altered configuration. The silicone remained stable throughout the testing, and a 50% increase in glass stresses was noted when comparing various "degraded" configurations. However, even at the maximum recorded stress during the 72-mm Crescendo test (2.1% drift), the utilization factor remained below 10%. When analysing the results from the Crescendo tests conducted both before and after the silicone damage occurred for the same unit (i.e., in the *Modified* frame configuration, created after the test sequence involving increasing artificial cuts), the recorded strain values revealed a shift in the hierarchy of strength among the façade components. Before the silicone crack formation, the transom had the highest utilization factor, followed by the mullion and glass (Figure 8c). After the crack appeared, the glass panel's strain increased significantly, making it the second highest in utilization after the transom. This might lead to an increased probability of glass fracture for higher intensity levels, as discussed in the following section.

3.3 | Performance Assessment

The façade performance was evaluated in terms of both serviceability and observed damage states. Post-earthquake serviceability tests were carried out in Phases 1 and 2 to assess the drift level at which the façade is no longer weather tight. These tests included air permeability, water penetration (Figure 9a) and wind resistance, conducted before and after exposure to low-to-moderate seismic intensities, as outlined in Table 3.

Initially, façade specimens (2, 3 in Table 2) underwent performance tests under pre-seismic conditions. These tests evaluated air leakage against acceptable rates for class A4 facades (EN 12153 [36]), ensured no water leakage was visible, and measured OOP deflections on both glass and frame to confirm they complied with normative deformation limits (18 mm for glass and 16 mm for frame, as per UNI EN 13830 [29] and UNI 11463 [41]). Air leakage tests were conducted both with the design configuration (assessing air permeability per unit length of joints) and with a fixed configuration (taped joints as shown in Figure 9b, assessing permeability per unit area of panels). After applying seismic intensity levels of 0.36% and 0.71% drift ratio, results showed that air tightness was maintained, with variations in air permeability rates up to 30% for suction and 25% for pressure, but the façade remained within the A4 classification limits. In terms of water tightness, drops of water were observed at 900 Pa after reaching the 0.71% drift level, indicating a loss of functionality for the façade (Figure 9c). For wind resistance, despite the expected noise in the suction phase due to the presence of the openings, frontal deflections measured by transducers at the middle of the frame and glass increased but remained within normative limits, with maximum recorded displacements of 9 mm.

Various structural-related damage states were observed during the entire experimental campaign, as summarized in Table 6. In Phase 1, the tested specimens showed good performance due to their construction detailing and internal gaps, with no significant damage mechanisms observed up to the maximum considered drift level of 0.71%. The only marginal damage noted during disassembly was the distortion of the anti-buckling components

TABLE 6 | Damage states observed during the whole experimental campaign.

Testing phase	Frame config.	Drift level	Observed damage	Damage description
Phase 1	Original	0.7%		Distortion of the anti-buckling components between the vertical mullions
Phase 2	Original	1.4%		Local deformations of the alignment block and surrounding areas
		5.2%		Dislodgement of the façade unit from its upper hook-bracket connection
Phase 3	Original	2.2%	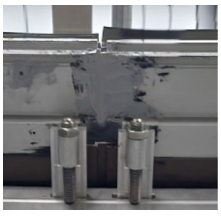	Damage to the silicone weatherseal between two SSG façade units
	Modified	3.5%		Damage to the structural silicone joint between glass and frame
		5.9%	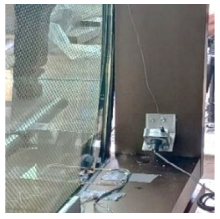	Detachment of glass panel after silicone failure in the corner
		6.7%		Permanent deformation of aluminium frame at the starter sill-bottom transom connection

(a) (b) (c)

FIGURE 9 | (a) Water resistance tests for specimen 1+3-T2, demonstrating the external water spray system with nozzles arranged on a grid to ensure uniform wetting of the specimen; (b) taped joints along the internal frame; (c) water drops indicating serviceability loss at 0.71% drift ratio.

located between the vertical mullions. In Phase 2, the failure modes of the T1-3 façade specimen were investigated. Apart from local deformations of the alignment block noticed during disassembly, the dislodgement of the façade unit from its upper bracket connection was observed at 174 mm (5.2% drift level) during the monotonic tests. This dislodgement resulted from the uplifting of the façade in the hook-bracket connection, which exceeded the maximum designed slot in the steel channel. In Phase 3, further investigations into the failure modes of the tested SSG units were conducted. After preliminary calibration tests on the façade units, it was observed that the bearing of the alignment screw on the starter sill caused the bottom transom to slide horizontally (as already observed in Galli [32]). This occurred because the design did not account for large movements for the specific real-world façade project. To address this, a spigot was bolted to the starter sill to allow higher displacement capacity of the frame for all T2 façade units, thus using this new design configuration for the experiments. As a result, the façade units (T2-1, T2-2) performed very well, with no structural damage observed under seismic loading. During the entire sequence, damage was only observed to the silicone weatherseal between two façade units at 75 mm (equivalent to a 2.2% drift value), followed by its failure at 100 mm (equivalent to a 2.9% drift value). However, this damage results in a serviceability loss for the façade, as damage to the silicone sheet indicates a loss of weather tightness.

As discussed above, to further study the impact of silicone joints on the results, cuts in the silicone were made (for specimen T1-2, Figure 10a) to simulate potential degradation caused by seismic events. The objective was to determine whether a compromised silicone joint, visible through a crack, needed to be secured to mitigate the risk of collapse during possible aftershocks [24]. These configurations ranged from 20% cracking, simulated by applying 100-mm cuts along the perimeter, to 80% cracking, where the cracks reached a length of 400 mm and were subjected to crescendo tests, with drift amplitudes reaching a maximum of 72 mm. Results highlight a consistent trend of increasing strain values and utilization factors for all the different components. The maximum values reached approximately 18% for the frame, 5% for the glass and 32% for the bracket. No propagation of artificially induced cracks was observed throughout the entire testing sequence.

The façade units in Phase 3 were then adjusted to simulate the *Modified* frame configuration, representing a design scenario characterized by limited deformation capacity of the frame. This was achieved by partially fixing the bottom transom in all the façade units (T2-1–4). This configuration resulted in higher stress on the silicone, causing cracking at 3.5% drift level as indicated in Table 6 (average value from all tested configurations in Phase 3). Upon cracking, the façade maintained its integrity and withstood additional shaking before failing due to glass detachment at higher drift ratios (increased by a factor 1.7). Although the silicone joints failed, this did not lead to a catastrophic failure of the unit, suggesting that the overall safety was not compromised until a 5.9% drift level. The silicone failure led to overall relative displacements of 8–12 mm between the glass and frame across the different units, with higher values for the 9 × 9 silicone aspect ratio, as recorded by the adhesive rulers (Figure 10b). This resulted in increased utilization factors in the glass panels, with a decreasing trend in response as the silicone aspect ratios increased, as shown in Figure 10c. The same figure also includes the value (red dot) observed for façade T1-3 (3.13 aspect ratio), where a value lower than 5% was recorded at the failure associated with the unit dislodgement. Furthermore, it was observed that the loading type affected the drift levels corresponding to the achievement of silicone failure. This damage state occurred at a similar drift level (3.5%) for the configurations subjected to monotonic loading. However, in the case of unit T2-3, failure occurred at a lower drift level (2.9%) during the application of the earthquake input (Table 2). This further underscores the potential significant influence of dynamic effects on the damage states definition.

3.4 | Discussion on Façade Damage States

The experimental tests have provided valuable insights into the damage states of unitized curtain wall facades. In particular, it was observed that the design of the frame system significantly influences the expected outcomes. The results obtained from the

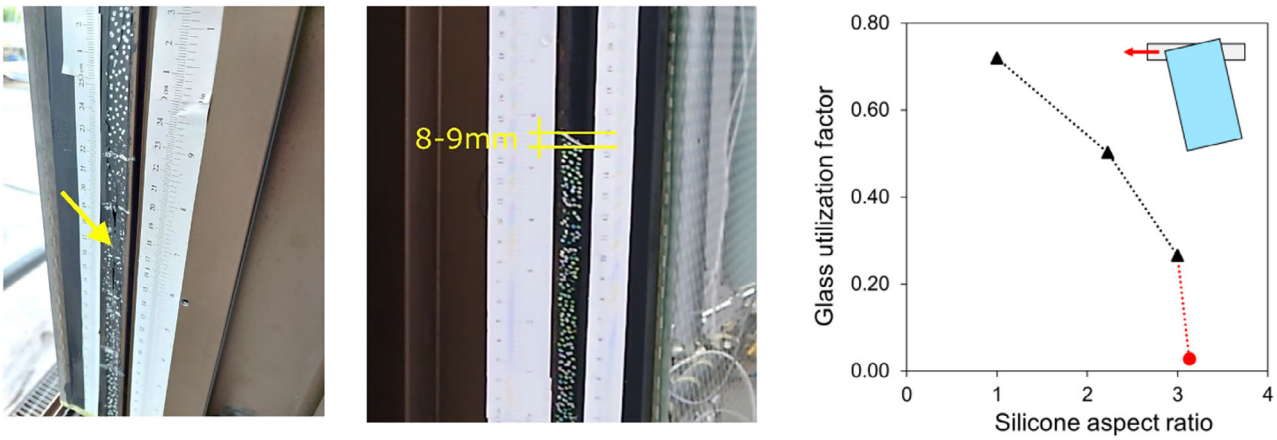

FIGURE 10 | (a) 20% artificial cut applied in the corner and then extended to the entire facade perimeter (along both mullions and transoms); (b) glass–frame relative displacement at the silicone failure at 3.87% drift level for T2-1; (c) glass utilization factors versus silicone aspect ratio at failure (red dot indicates the value for T1-3).

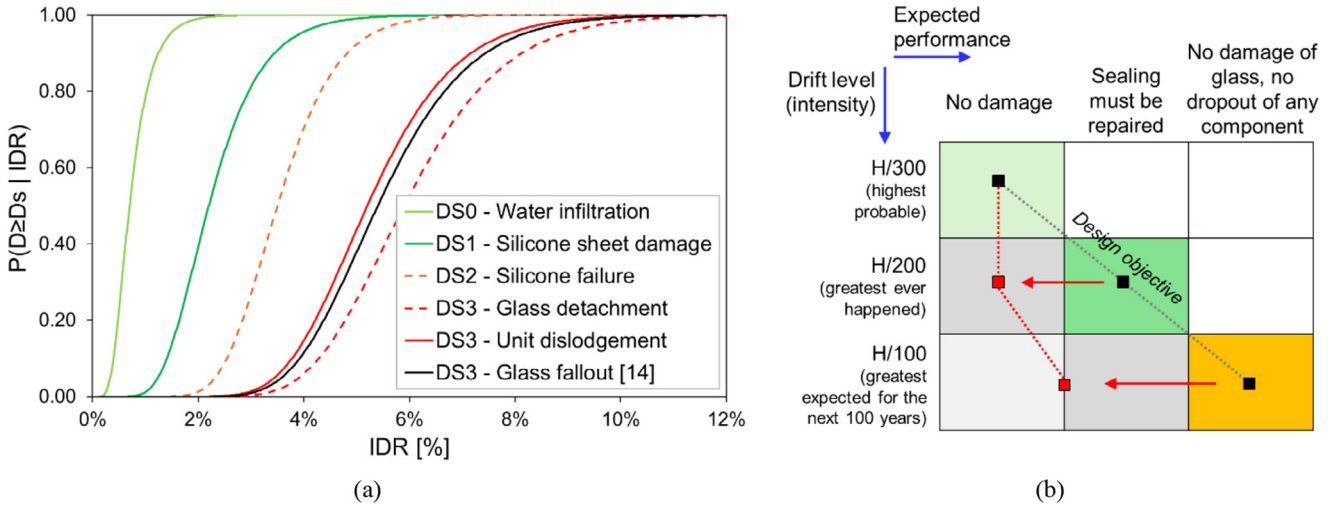

FIGURE 11 | (a) Fragility curves elaborated from the experimental results, including literature data for DS3. (b) Design objective level (black dots) according to JASS14 [30] versus measured façade performance (red dots).

experimental campaign have then been further elaborated for the purpose of assessing the seismic vulnerability by developing fragility curves for use in risk assessment studies. Fragility curves were derived using the following equation (Equation 1), proposed by Porter et al. [42]:

$$P(D_s \geq D_{sx}|\mathrm{IDR}) = \Phi\left(\frac{\ln\left(\frac{\mathrm{IDR}}{x_m}\right)}{\beta}\right) \quad (1)$$

The fragility curve is represented by a log-normal distribution, defining the probability of the non-structural element exceeding a damage state D_{sx} (e.g., D_{S1}, D_{S2}, D_{S3}) given a specific inter-storey drift ratio (IDR), which is the engineering demand parameter. The function Φ represents the standard normal distribution, with x_m and β as the mean and standard deviation, respectively. Figure 11a shows the fragility curves obtained for both serviceability and failure modes, where the dispersion values were assumed equal to 0.45 for D_{S0} and D_{S1}, while 0.25 for D_{S2} and D_{S3}. These dispersion values were based on existing fragility data for unitized curtain walls [17], given the limited recorded data. Figure 11a highlights that non-structural damage states (water infiltration, damage to the silicone sheet between vertical units) significantly impact the façade behaviour at lower drift levels. At higher drift levels, although damage initiates earlier in configurations with limited frame displacement capacity (dashed curves), the ultimate failure of the façade system (D_{S3}) occurs at similar drift ratios for the *Original* (continuous red curve) versus *Modified* (dashed red curve) configurations. The graph also includes a fragility curve for glass fallout (representing a D_{S3}) from the literature (black curve), showing its alignment with the experimental results discussed in this paper.

Fragility curves further confirm the excellent seismic performance of unitized curtain walls, which are expected to fail at very high drift ratios, thereby demonstrating their seismic resilience. When considering the performance objectives typi-

cally assessed in seismic certification tests, it is evident that the façade specimens perform very well at low-to-moderate intensity levels. Their performance exceeded the expectations outlined by JASS14 [30] (Figure 11b). However, it is important to note that the design objectives defined by codes/guidelines should also encompass non-seismic performance criteria. This includes addressing potential functionality losses, such as water infiltration and air permeability to define comprehensive multi-performance objectives and design targets. Regarding high-intensity levels, international codes do not impose a clear limit for verifying the demand versus expected façade performance at such levels. Nevertheless, under the *Original* configuration, the façade showed a low probability of damage when considering the maximum drift level specified by AAMA 501.6 [33] for safety checks, which is approximately a 4.4% drift ratio for the tested façade specimens.

4 | Conclusions

This paper presents an experimental investigation into the seismic performance of full-scale unitized glazed curtain walls. The experiments were part of a research project which aimed to (i) assess the performance of these facades comprehensively, by defining the seismic demand levels at which functionality and structural damage or failure occur; (ii) establish the impact of façade construction details, such as glass type, joints and frame design, on seismic behaviour and (iii) calibrate numerical models that support component-level studies of unitized curtain walls. To achieve these objectives, a series of experimental tests was conducted on various façade specimens. These specimens included different aspect ratios for glass and spandrel panels, both dry-glazed and wet-glazed joints and frames designed with either high or limited displacement capacities. The paper provides detailed descriptions of the façade specimens and the test setup, which involved quasi-static and dynamic tests of increasing intensity levels. Additionally, tests for air infiltration, water leakage and wind resistance were conducted before and after low-intensity seismic tests to evaluate the post-earthquake façade serviceability performance.

Based on observations and the analysis of experimental data, the following main conclusions were drawn:

- The IP behaviour of the façade varied depending on the direction of movement—positive or negative—due to the position of the alignment screw/block and the asymmetric restraint conditions of the curtain wall unit, which either allowed rotational movement or induced deformation.
- In wet-glazed units, the glass response was strongly influenced by the silicone properties, with lower silicone aspect ratios leading to increased glass rotation. A 30% reduction in rotation was observed when the silicone aspect ratio was increased from 1.00 to 2.22. The silicone behaviour also significantly influenced the strength hierarchy within the façade. This effect was particularly evident in configurations with cracked silicone, where the likelihood of glass fracture increased at higher loading intensities.
- When comparing results across different seismic directions, rotations induced by vertical IP loading were relatively limited; however, frame diagonal elongation and deformation were notably affected. OOP horizontal shaking led to unit rotations roughly twice as large as IP loading, due to hinge connections and greater façade flexibility.
- The dynamic effects on the façade were particularly evident when comparing cyclic and time-history loading. Dynamic loads resulted in component displacements that were nearly 1.5 times lower than those observed under quasi-static cyclic loading. This reduction can be attributed to the damping properties of the silicone and the internal gaps, which influence the load distribution within the unit.
- The post-earthquake serviceability tests revealed that the façade maintained air tightness and wind resistance following low-to-moderate seismic events. However, weather-tightness was compromised at a drift level of 0.71%, as evidenced by water leakage at 900 Pa.
- The façade units performed well under seismic loading, with no significant structural damage observed in most cases. The frame detailing had a notable impact on the outcomes. Frames with limited displacement capacity led to silicone failure, but the overall integrity of the façade was preserved until reaching high drift levels. In contrast, configurations with frames designed for higher displacement capacities, ultimate failure occurred due to the dislodgement of a façade unit at drift levels exceeding 5%.

The experimental tests demonstrated that unitized curtain wall facades exhibit strong seismic resilience, with failure occurring only at very high drift ratios. The development of fragility curves from the test data supports this conclusion, showing that while non-structural damage—such as water infiltration and silicone weatherseal damage—can occur at lower drift levels, the overall structural integrity of the facades is preserved even at higher displacements. However, these results highlight the need to consider multi-performance hazard criteria in design to ensure both safety and functionality during and after seismic events. Although the study provides insights into the overall performance of unitized curtain walls and the impact of design choices, further research is needed. Future investigations should focus on comparing the findings with design criteria specified by current standards and practices, in particular, the effects of joint design. To fully understand the record-to-record variability and its impact on the facade system, studies involving a larger set of signals and supported by numerical modelling are needed. Finally, data from Digital Image Correlation measurements on glass and silicone, along with additional testing, could help develop more robust fragility curves.

Acknowledgements

This study has received funding from the European Union's Horizon 2020 research and innovation programme under the Marie Skłodowska-Curie grant agreement No. 101029605 (H2020-MSCA-IF-2020–SAFE-FACE—Seismic SAFety and Energy efficiency: Integrated technologies and multi-criteria performance-based design for building FACadEs) for Simona Bianchi. The authors also acknowledge the valuable contribution and support provided by Permasteelisa and, in particular, by Matteo Dazzan, Test & Lab specialist, Gianluca Casagrande, I&T specialist of the experimental measurement acquisition system and all the Test&Lab members.

Data Availability Statement

The data that support the findings of this study are available from the corresponding author upon request.

References

1. S. Murray, *Contemporary Curtain Wall Architecture* (Princeton Architectural Press, 2009).

2. T. Klein, *Integral Facade Construction—Towards a New Product Architecture for Curtain Walls* (Architecture and the Built Environment, 2013).

3. R. Hartwell, S. Macmillan, and M. Overend, "Circular Economy of Façades: Real-World Challenges and Opportunities," *Resources, Conservation and Recycling l* 175 (2021): 105827, https://doi.org/10.1016/j.resconrec.2021.105827.

4. R. Hartwell and M. Overend, "Reclamation Potential in the Built Environment: A Method and Metric for Assessing Environmental Benefits Beyond First Use," *Building and Environment* 263 (2024): 111866, https://doi.org/10.1016/j.buildenv.2024.111866.

5. D. Evans and F. J. Lopez Ramirez, "Glass Damage in the 19 September 1985 Mexico Earthquake," in *Reducing Earthquake Hazards: Lessons Learned From the 1985 Mexico Earthquake* (V. Bertero, 1989).

6. E. Miranda, G. Mosqueda, R. Retamales, and G. Pekcan, "Performance of Nonstructural Components During the 27 February 2010 Chile Earthquake," *Earthquake Spectra* 28, no. S1 (2010): S453–S471, https://doi.org/10.1193/1.4000032.

7. A. Baird, A. Palermo, and S. Pampanin, "Facade Damage Assessment of Multi-Storey Buildings in the 2011 Christchurch Earthquake," *Bulletin of the New Zealand Society for Earthquake Engineering* 44, no. 4 (2011): 368–376, https://doi.org/10.5459/bnzsee.44.4.368-376.

8. S. Bianchi and S. Pampanin, "Fragility Functions for Architectural Nonstructural Components," *ASCE Journal of Structural Engineering* 148, no. 10 (2022): 03122005, https://doi.org/10.1061/(ASCE)ST.1943-541X.0003352.

9. B. Huang, S. Chen, W. Lu, and K. M. Mosalam, "Seismic Demand and Experimental Evaluation of the Nonstructural Building Curtain Wall: A Review," *Soil Dynamics and Earthquake Engineering* 100 (2017): 16–33, https://doi.org/10.1016/j.soildyn.2017.05.025.

10. M. Momeni and C. Bedon, "Review on Glass Curtain Walls Under Different Dynamic Mechanical Loads: Regulations, Experimental Methods and Numerical Tools," *Façade Design - Challenges and Future Perspective* (Intech Open, 2024), https://doi.org/10.5772/intechopen.113266.

11. J. G. Bouwkamp, "Behavior of Window Panel Under In-Plane Forces," *Bulletin of the Seismological Society of America* 51, no. 1 (1961): 85–109, https://doi.org/10.1785/BSSA0510010085.

12. J. G. Bouwkamp and J. F. Meehan, "Drift Limitations Imposed by Glass," in *2nd World Conference on Earthquake Engineering* (1960).

13. K. Broker, S. Fisher, and A. Memari, "Seismic Racking Test Evaluation of Silicone Used in a Four-Sided Structural Sealant Glazed Curtain Wall System," *Journal of ASTM International* 9, no. 3 (2012): 104144, https://doi.org/10.1520/JAI104144.

14. X. Ji, Y. Zhuang, W. Lim, and Z. Qu, "Seismic Behavior of a Fully Tempered Insulating Glass Curtain Wall System Under Various Loading Protocols," *Earthquake Engineering & Structural Dynamics* 53 (2024): 68–88, https://doi.org/10.1002/eqe.4017.

15. W. Lu, B. Huang, K. M. Mosalam, and S. Chen, "Experimental Evaluation of a Glass Curtain Wall of a Tall Building," *Earthquake Engineering & Structural Dynamics* 45, no. 7 (2016): 1185–1205, https://doi.org/10.1002/eqe.2705.

16. A. M. Memari, N. Simmons, and R. L. Solnosky, "Unitized Curtain Wall Systems Joint Performance With Re-Entrant Corners Under Seismic Racking Testing," *Journal of Building Engineering* 40 (2021): 102715, https://doi.org/10.1016/j.jobe.2021.102715.

17. A. M. Memari, W. C. O'Brien, K. J. Hartman, P. A. Kremer, and R. A. Behr, Architectural Glass Seismic Behavior Fragility Curve Development, Background Document FEMA P-58/BD-3.9.1 ATC (2011).

18. F. A. Arifin, T. J. Sullivan, and R. P. Dhakal, "Experimental Investigation Into the Seismic Fragility of a Commercial Glazing System," *Bulletin of the New Zealand Society for Earthquake Engineering* 15, no. 3 (2020): 144–149, https://doi.org/10.5459/bnzsee.53.3.144-149.

19. L. Casagrande, A. Bonati, A. Occhiuzzi, N. Caterino, and F. Auricchio, "Numerical Investigation on the Seismic Dissipation of Glazed Curtain Wall Equipped on High-Rise Buildings," *Engineering Structures* 179 (2019): 225–245, https://doi.org/10.1016/j.engstruct.2018.10.086.

20. N. Caterino, M. Del Zoppo, G. Maddaloni, A. Bonati, G. Cavanna, and A. Occhiuzzi, "Seismic Assessment and Finite Element Modelling of Glazed Curtain Walls," *Structural Engineering and Mechanics* 61, no. 1 (2017): 77–90, https://doi.org/10.12989/sem.2017.61.1.077.

21. S. D'Amore, S. Bianchi, J. Ciurlanti, and S. Pampanin, "Seismic Assessment and Finite Element Modeling of Traditional vs Innovative Point Fixed Glass Facade Systems (PFGFS)," *Bulletin of Earthquake Engineering* 21 (2023): 2657–2689, https://doi.org/10.1007/s10518-023-01622-0.

22. N. Cella and C. Bedon, "Numerical Modelling of Global/Local Mechanisms and Sensitivity Analysis for the Seismic Vulnerability Assessment of Glass Curtain Walls," *Engineering Structures* 319 (2024): 118859, https://doi.org/10.1016/j.engstruct.2024.118859.

23. J. Kimberlain, V. Hayez, J. Feng, and M. Mirgon, "SSG and Seismic Design Boundaries in Advanced Modeling," in *Facade Tectonics 2022 World Congress* (2022).

24. V. Hayez, S. Bianchi, G. Lori, J. Feng, and J. Kimberlaind, "Performance of Silicone Bonded Facades During Seismic Events," in *Glass Performance Days* (2023).

25. J. Ciurlanti, G. Milan, J. Dennis, et al., "Sensitivity Analysis and Risk Assessment of Unitised Glass Curtain Walls," in *SECED 2023 Conference* (2023).

26. D. A. Nuñez Enriquez, "Seismic Performance of Glazed Curtain Walls Connections: Experimental Testing and Finite Element Modelling" (MSc thesis, Delft University of Technology, 2022).

27. E. Stavridou, "Simulation of the Overall Performance of Glazed Unitised Curtain Walls Under Seismic Action Through Finite Element Modelling and Validation via Full-Scale Experimental Testing" (MSc thesis, Delft University of Technology, 2023).

28. EN 1998-1, *Eurocode 8: Design of Structures for Earthquake Resistance—Part 1 - General Rules* (Seismic Actions and Rules for Buildings, 2004).

29. UNI EN 13830, *Curtain Walling—Product Standard* (European Committee for Standardization, 2022).

30. JASS14, *Japanese Architectural Standard Specification Curtain Wall* (Architectural Institute of Japan, 1996).

31. EAD 090010-00-0404, Bonded Glazing Kits and Bonding Sealants European Assessment Document (EOTA, 2018).

32. U. Galli, "Seismic Behaviour of Curtain Wall Facades—a Comparison Between Experimental Mock-Up Test and Finite Element Method Analysis" (MSc thesis, Technical University of Milan, 2011).

33. AAMA 501.6-09, *Recommended Dynamic Test Method for Determining the Seismic Drift Causing Glass Fallout From a Wall System* (American Architectural Manufacturers Association, 2009).

34. NTC, *Ministero Delle Infrastrutture*, Aggiornamento Delle Norme Tecniche per le Costruzioni. Supplemento ordinario n°8 alle G.U. n° 42 del 20/02/2018 (2018).

35. J. Ciurlanti, S. Bianchi, and S. Pampanin, "Raising the Bar in Seismic Design: Cost–Benefit Analysis of Alternative Design Methodologies and Earthquake-Resistant Technologies," *Bulletin of Earthquake Engineering* 21, no. 5 (2023): 2723–2757, https://doi.org/10.1007/s10518-023-01625-x.

36. EN 12153, *Curtain Walling—Air Permeability—Test Method* (European Committee for Standardization, 2023).

37. EN 12155, *Curtain Walling—Watertightness—Laboratory Test Under Static Pressure* (European Committee for Standardization, 2000).

38. EN 12179, *Curtain Walling—Resistance to Wind Load* (European Committee for Standardization, 2000).

39. S. Bianchi, G. Lori, V. Hayez, M. Overend, and G. Manara, "Influence of Design Variables on Seismic Performance of Unitized Curtain Walls: A Parametric Experimental Study," *Glass Structures & Engineering* 9, no. 2 (2024): 165–184, https://doi.org/10.1007/s40940-024-00255-2.

40. W. C. O'Brien, A. M. Memari, P. A. Kremer, and R. A. Behr, "Fragility Curves for Architectural Glass in Stick-Built Glazing Systems," *Earthquake Spectra* 28, no. 2 (2012): 639–665, https://doi.org/10.1193/1.4000011.

41. UNI 11463, *Glass in Building—Determination of the Load Resistance of Flat Glass Panes Applied as Infill Panels—Calculation Method* (European Committee for Standardization, 2016).

42. K. Porter, R. Kennedy, and R. Bachman, "Creating Fragility Functions for Performance-Based Earthquake Engineering," *Earthquake Spectra* 23, no. 2 (2007): 471–489, https://doi.org/10.1193/1.2720892.